Length distributions in metallic alloys

Normand Mousseau and M. F. Thorpe
Department of Physics and Astronomy and Center for Fundamental Materials Research, Michigan State University, East Lansing, Michigan 48824
(Received 26 June 1991)

We use the embedded-atom potential of Johnson to compute the length-distribution functions for a large number of fcc binary metallic alloys. From these distributions, we extract the mean lengths of the nearest-neighbor bonds, which compare well with recent extended x-ray-absorption fine-structure (EXAFS) experiments in Ni_xAu_{1-x}. In other cases, where EXAFS results are not available, we compare our results with the mean lattice parameter as determined by diffraction experiments. While the embedded-atom potential is accurate for some alloys (e.g., Ni-Au), we show that for alloys containing Pt, a simple central-force model is superior. The embedded-atom potential of Johnson predicts an unexpected contraction of the Au-Au distance in Ag-rich Au-Ag alloys. We point out that an important characteristic of any alloy potential is its ability to get the single and double defects correct.

I. INTRODUCTION

In the last few years, the problem of length mismatch in alloys has received considerable attention both theoretically and experimentally. Thorpe and co-workers[1,2] have recently solved this problem analytically for alloys with equal harmonic spring interactions between nearest-neighbor atoms, joined by bonds with different natural lengths. Experimentally, the development of extended x-ray-absorption fine-structure spectroscopy (EXAFS) has provided more information concerning the near-neighbor lengths in alloys. These lengths are of primary importance for a proper structural characterization and in understanding the deviations from Vegard's law, which states that the mean lattice parameter varies linearly with the composition.[3]

From this point of view, the study of fcc binary metallic alloys is very interesting since for these compounds, the deviations from Vegard's law are much more significant than, for example, in semiconductors.[2] The development of the embedded-atom-method (EAM) potentials[4,5] which have given reliable results for the energies of pure metals, with and without impurities, and binary alloys,[4,6] makes it possible to take into account, in a simple way, some of the electronic effects. The EAM potentials are, in general, fast to compute, allowing the use of very large supercells, which is important when trying to extract statistical information from random alloys. The version chosen for the present study is the Johnson EAM potential,[7–9] developed recently and possessing two major advantages over other EAM potentials: (1) it is completely analytic and (2) it requires *no additional parameters* for the alloy once the parameters for the pure metals are fixed. The lack of additional alloy parameters has ultimately proved to be a problem for us, as there are no adjustable parameters to fit experiment. In this paper we show that the Johnson EAM potentials are remarkably good in some cases (e.g., Ni_xAu_{1-x}) but quite unsatisfactory in others (e.g., alloys containing Pt).

Deviations from Vegard's law for metallic alloys have been known since the beginning of x-ray measurements more than 60 years ago. Until recently, however, Vegard's law was actually nothing more than an *ad hoc* assumption,[3] but it has been shown that Vegard's law is to be expected only in those cases where there is length mismatch accompanied by *no* changes in the force constants.[1,2] As these conditions never occur in reality, the discussion must always be about the magnitude and sign of the deviations from Vegard's law. These deviations are small in semiconductors,[10] but can be much larger in metals. During the fifties, a few models were proposed to quantify these deviations,[11] but they all started with the assumption that the solid solution forms a perfect network, i.e., all the lengths are identical.

In this paper we present computer simulation results from the EAM potential. We also present both analytic and computer simulation results from a much simpler spring model. This central force model (CFM) uses only nearest-neighbor central forces between an atom and its 12 neighbors. It has the virtue that it can be solved analytically in some cases, and can be used in conjunction with the EAM results to assess the sensitivity of the results to the local environment. The CFM is completely independent of the local configuration and incorporates the transferability of the force constants for a particular type of bond to all environments. On the other hand the EAM effectively modifies the force constants of a particular bond in response to the local environment around that bond. This is accomplished via the embedding function. We shall refer to this effect as *charge transfer* in the rest of this paper. We show that the EAM potential gives results in reasonable agreement (better than CFM) with experiment for most of the binary alloys composed of Ag, Au, Cu, Ni, and Pd while alloys containing Pt all deviate strongly from the EAM results. In this paper we use EAM to refer to the Johnson EAM, and note that other versions of the EAM for alloys may well give different results. Surprisingly, we observe that the CFM gives good

agreement with experimental diffraction data for the Ni-Cu, Pd-Ag and all Pt alloys. These results suppose, as we will see in Sec. V, that the charge transfer is least important for alloys containing Pt where we can treat the atoms as rigid objects connected by elastic springs. We also present some analytic and computer results for the bond-length distributions in alloys. The general features of these distributions are not, in general, very sensitive to the particular model and are found to be remarkably wide, of the order of the length mismatch itself.

Another quantity of interest is the variation of the elastic constants with concentration. We have computed the bulk and shear moduli and find that these quantities are also rather insensitive to the model used. In particular, both the EAM and the CFM show very similar results for the bulk modulus. As there are almost no experimental results available for the elastic moduli in bulk alloys, the results we present here must be considered as predictions to be confirmed or otherwise by future experiments.

II. EMBEDDED-ATOM METHOD

As we already mentioned, the Johnson version of the EAM[8] potential was used for our simulations, and we will summarize this below. In EAM, the electron-density functions are only determined to within a scaling factor. For pure metals, this factor rescales the embedding function. But the situation is very different in alloys where the relation between the electron density of the two components strongly affects the mixing energies.[6] The interest in the Johnson potential is that it is completely analytic and requires no extra parameter for the alloys. All the parameters are determined using the atomic volume, the cohesive energy, the bulk modulus, the average shear modulus, and the vacancy-formation energy for the pure metals. The approximation used by Johnson is based on the preservation of the invariance of the energy under a gauge transformation involving the embedding function and the pair potential. This choice of constraint is of course as arbitrary as the arithmetic mean used by Foiles,[6] but has the advantage of being fairly *natural* within the EAM formalism. In the notation used by Johnson,[7] the EAM potential is defined by

$$E_t = \sum_i F^i(\rho_i) + \tfrac{1}{2}\sum_{i,j}{}'\Phi^{ij}(r_{ij}), \quad \rho_i = \sum_j{}' f^j(r_{ij}), \tag{1}$$

where E_t is the total internal energy, ρ_i is the total electronic density due to neighbors j at site i, $F(\rho_i)$ is the embedding energy for atom i, and $\phi(r_{ij})$ is a repulsive ion-ion core pair potential. The prime on the summations indicates that the self-terms $i = j$ are excluded. The functions used in the potential are defined as follows:

$$\Phi^{ij}(r) = \frac{1}{2}\left(\frac{f^i(r)}{f^j(r)}\phi^j(r) + \frac{f^j(r)}{f^i(r)}\phi^i(r)\right) \tag{2}$$

and

$$F^i(\rho) = -E_c^i\left(1 - \ln\left[\left(\frac{\rho}{\rho_e^i}\right)^{\alpha'/\beta'}\right]\right)\left(\frac{\rho}{\rho_e^i}\right)^{\alpha'/\beta'} - 6\phi_e^i\left(\frac{\rho}{\rho_e^i}\right)^{\gamma'/\beta'}, \tag{3}$$

where

$$f^i(r) = f_e^i \exp\left[-\beta^i(r/r_e^i - 1)\right] \tag{4}$$

and

$$\phi^i(r) = \phi_e^i \exp\left[-\gamma^i(r/r_e^i - 1)\right]. \tag{5}$$

The parameters used in this paper are the same as those given by Johnson[8] and are shown in Table I.

The EAM potential for pure metals is not restricted by the isotropy relation $C_{11} = 2C_{44} + C_{12}$ of the CFM, which is rarely obeyed in metals. However the EAM potential does only allow two independent elastic constants, and as a result imposes the general EAM condition $C_{11} = C_{44} + C_{12}$ which *is* reasonably well obeyed for many fcc metals.[12] We find (numerically) that the relation $C_{11} = C_{44} + C_{12}$ still holds for alloys, so that there are only two, instead of three, independent elastic constants. As the bulk modulus $B = [C_{11} + 2C_{12}]/3$ and the Voight average shear constant $G = [3C_{44} + (C_{11} - C_{12})]/5$ are fitted in the EAM potential for the pure metals, we use these as the two independent elastic constants for the alloy.

III. CENTRAL FORCE MODEL

In order to get an idea of the importance of the redistribution of the electronic charges in the alloy, and to gain some perspective on the EAM model, we have compared the results of the EAM potential with a simple nearest-neighbor spring model (CFM).[1] The total energy for an $A_{1-x}B_x$ alloy is given by

TABLE I. Parameters for the Johnson EAM potential. Ω is the atomic volume (Å^3), and only the ratios of the f_e are relevant and the other parameters are dimensionless.

Atom	Ω	f_e	ϕ_e	α	β	γ
Cu	11.81	0.30	0.59	5.85	5.85	8.00
Ag	17.10	0.17	0.48	5.92	5.96	8.26
Au	16.98	0.23	0.65	6.37	6.67	8.20
Ni	10.90	0.41	0.74	4.98	6.41	8.86
Pd	14.72	0.27	0.65	6.42	5.91	8.23
Pt	15.06	0.38	0.95	6.44	6.69	8.57

$$E = \frac{1}{2} \sum_{<i,j>} K_{ij} \left(L_{ij} - L_{ij}^{o}\right)^2, \tag{6}$$

where the A-A and B-B spring constants and equilibrium lengths are taken from the parameters for the pure metal as given by Johnson,[8] and the additional alloy parameters are chosen to be

$$K_{AB} = \frac{2K_{AA}K_{BB}}{K_{AA} + K_{BB}}, \tag{7}$$

which corresponds to adding half springs in series. The natural (*unstrained*) lengths are

$$L_{AB}^{0} = \frac{1}{2}\left(L_{AA}^{0} + L_{BB}^{0}\right). \tag{8}$$

The angular brackets in the summation in Eq. (6) indicate that each nearest-neighbor bond is only counted once. The spring constants are functions of the bulk modulus B and the nearest-neighbor distance L^0 (Ref. 13)

$$K = \frac{3L^0}{2\sqrt{2}}B. \tag{9}$$

The mean and variance of the bond-length distribution become particularly transparent within the CFM when *all the force constants are equal* as the model can be solved analytically. The mean lengths and their variances can be expressed as a function of a^{**}, the topological rigidity parameter,[1,2] defined in terms of the radial force on the 12 nearest neighbors, required to open up a cage:

$$F = \frac{K}{a^{**}}u, \tag{10}$$

where u is the resulting radial displacement. The topological rigidity parameter $0 < a^{**} < 1$ can be computed as a lattice integral. It is zero for a perfectly rigid lattice, and unity for a completely floppy matrix. In semiconductors, because of the low coordination and weak angular forces, a^{**} varies from 0.70 to 0.82,[2,14] while in fcc metals we find that $a^{**} = 0.24$.[15] The mean lengths are found to be

$$< L >= (1-x)L_{AA}^{0} + xL_{BB}^{0}, \tag{11}$$

$$< L_{AA} >=< L > + xa^{**}(L_{AA}^{0} - L_{BB}^{0}), \tag{12}$$

$$< L_{BB} > - < L_{AA} >= a^{**}(L_{BB}^{0} - L_{AA}^{0}), \tag{13}$$

and

$$< L_{AB} >= \frac{1}{2}(< L_{AA} > + < L_{BB} >), \tag{14}$$

with the variances of the distributions are given by[2,15]

$$\begin{aligned} &< L_{AA}^2 > - < L_{AA} >^2 \\ &\quad =< L_{BB}^2 > - < L_{BB} >^2 \\ &\quad =< L_{AB}^2 > - < L_{AB} >^2 \\ &\quad = \frac{1}{2}x(1-x)a^{**}(1-a^{**})(L_{BB}^{0} - L_{AA}^{0})^2. \end{aligned} \tag{15}$$

The equations for $K_{AA} = K_{AB} = K_{BB}$ are not used in this paper, except in constructing Fig. 11 and for a limiting case in the Appendix.

The CFM defined by (7) and (8) can be solved exactly in the dilute limit as shown in the Appendix.

It is also possible to find the effective elastic constant K_e by an effective-medium theory[14] when the force constants vary. It can be shown within the CFM that the equations for the lengths and spring constants decouple so that the effective spring constant K_e is independent of the length mismatch. From effective medium theory,[1,13,14] and using the relation (7), we have

$$\frac{(1-x)(K_{AA} - K_e)}{K_e(1-p_I) + K_{AA}p_I} + \frac{x(K_{BB} - K_e)}{K_e(1-p_I) + K_{BB}p_I} = 0, \tag{16}$$

where $p_I = \frac{1}{2}(1 + a^{**})$ determines the initial slope for the conductance,[14,16] which obeys the same effective-medium equation as the spring constant. Equation (16) is a quadratic for K_e which always is sublinear and monotonic in the concentration x. As we will see in Sec. V, these analytical results are very close to the ones obtained with the EAM. The CFM is a very simple and crude model, but gives surprisingly good results for some of the alloys, particularly those containing Pt.

IV. COMPUTER SIMULATIONS

The computer simulation results shown in this paper for both the EAM and CFM have been obtained by statically minimizing the total energy using a conjugate-gradient algorithm. The simulations have been performed with 4000 atoms in an fcc arrangement with a cubic supercell and periodic-boundary conditions. In the relaxation, all the atoms were free to move and the volume of the supercell could change while remaining cubic. The elastic constants are computed by varying the shape and/or size of the unit cell appropriately and re-relaxing the system. This method leads to three figure accuracy, which is comparable or better than the available experimental results. It was found that the supercell was large enough that it was not necessary to do any ensemble averaging.

V. RESULTS

In Figs. 1–6 we compare the EAM and CFM computer simulation results with diffraction data where available and with EXAFS data for $Ni_{1-x}Au_x$ in Fig. 6. In Fig. 1 for Au-Ag, the EAM results agree extraordinarily well with diffraction data and are clearly superior to the CFM results. Because Au and Ag atoms have very similar sizes, we expected this case to be quite uninteresting as indeed the results are for the CFM. The experimental data show a minimum in the mean length at about $x \simeq 0.4$. Fournet,[11] using an elastic sphere approximation, predicted that the deviation from Vegard's law should be maximum for very small length mismatch but gave no number and was working in the virtual crystal approximation. As seen in Fig. 1, the EAM follows almost *exactly* the experimental data except at low con-

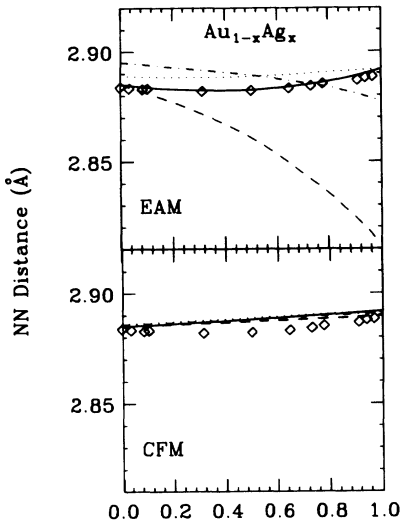

FIG. 1. The mean A-A, A-B, B-B nearest-neighbor distances and the lattice parameter are shown for the alloy $A_{1-x}B_x$. Dashes are for A-A distance; dot-dashes, for A-B distance; dots, for B-B distance; and the continuous line is for the mean distance. The symbols are experimental data. The upper panel is for the embedded atom method (EAM) and the lower panel is for the central force model (CFM). This figure is for $Au_{1-x}Ag_x$. The diffraction data for $Au_{1-x}Ag_x$ (Ref. 20) is shown as diamonds.

centration of Au, where the difference is only due to the fact that the lattice parameter of pure Ag has not been taken at the experimental temperature to fit the parameters for the EAM potential. For this alloy only, the simulation results have been obtained using a polynomial potential with a cut-off radius after the third shell of neighbors. This potential is very similar to the one described here; for more details see the paper by Johnson.[9] We used a longer range interaction for this alloy because

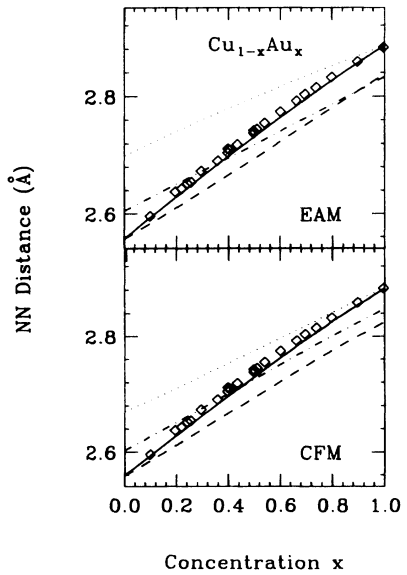

FIG. 2. Same as Fig. 1, except for $Cu_{1-x}Au_x$. The diffraction data for $Cu_{1-x}Au_x$ is shown as diamonds (Refs. 21 and 22).

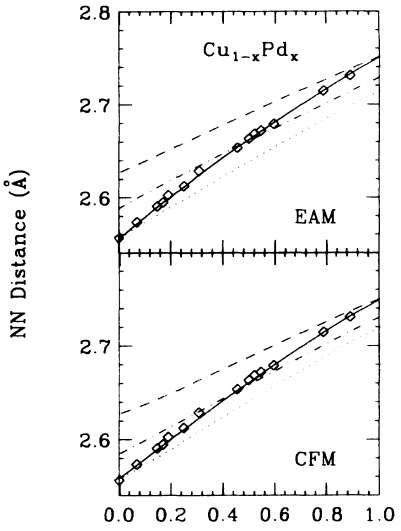

FIG. 3. Same as Fig. 1, except for $Cu_{1-x}Pd_x$. The diffraction data for $Cu_{1-x}Pd_x$ is shown as diamonds (Ref. 23).

Johnson mentioned that it is the only one which shows some change in energy with the range of interaction. All the other alloys studied here are quite stable under such a change.[9] We note that the condition $C_{11} = C_{12} + C_{44}$ is *not* obeyed in either the pure materials or the alloy due to the further neighbor interactions. It is worth mentioning that Ackland and Vitek[17] also see a minimum with their EAM potential but around $x \simeq 0.5$. The behavior of the Au-Au bond length in this alloy is quite strange; instead of becoming closer to the length of the Ag-Ag bond, it decreases by more than 0.07 Å (3%), close to 10 times the length mismatch. This behavior can be explained by looking at the parameters for the potential: the easiest way for the Au atom to satisfy its need for a

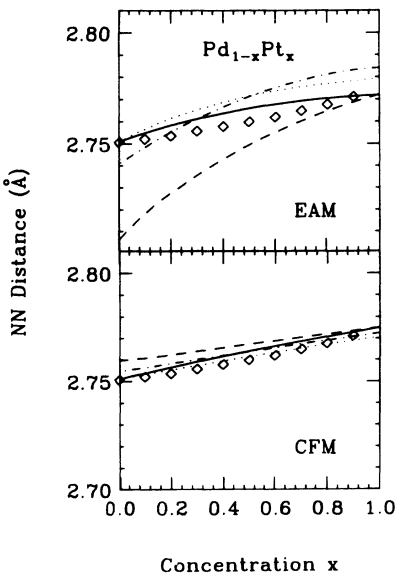

FIG. 4. Same as Fig. 1, except for $Pd_{1-x}Pt_x$. The diffraction data for $Pd_{1-x}Pt_x$ is shown as diamonds (Ref. 24).

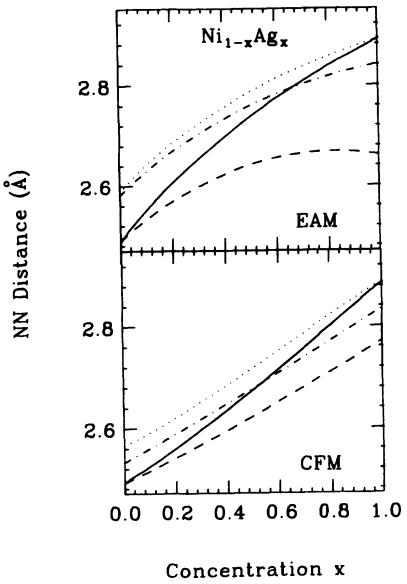

FIG. 5. Same as Fig. 1, except for $Ni_{1-x}Ag_x$.

large electronic density is to become closer to another Au atom. But, besides the mean length which agrees with the experiment, it is impossible to tell whether or not this behavior is real. As this behavior is probably too small to be discerned by EXAFS, only *ab initio* calculations, especially of Au-Au pairs in Ag, can give further insight into this phenomenon.

In Fig. 2, the results for Cu-Au alloys show that the EAM and CFM are about equally good, but do show systematic discrepancies with the diffraction results. The results for Cu-Pd in Fig. 3 give impressive agreement with the diffraction results for both EAM and CFM. The partial mean lengths are also similar, suggesting that charge transfer effects do not make much difference here. In contrast the results for Pd-Pt in Fig. 4 show that the CFM is superior to the EAM in reproducing the diffraction data. The CFM produces a very narrow range of mean lengths in this case with a minimal amount of bowing. The results of EAM and CFM are quite remarkably different in Ni-Ag as shown in Fig. 5, giving bowing with opposite signs. There is no experimental data on Ni-Ag as it phase separates.

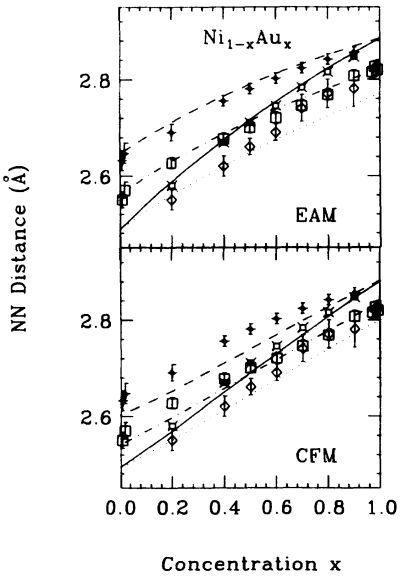

FIG. 6. Same as Fig. 1, except for $Ni_{1-x}Au_x$. The diffraction data for $Ni_{1-x}Au_x$ is shown as stars (Ref. 18). The EXAFS data, with error bars, is taken from Renaud *et al.* (Ref. 18). The diamonds, squares, and small circles refer to the Ni-Ni, Ni-Au, and Au-Au nearest-neighbor distances, respectively, and the stars are the mean lengths.

In Fig. 6 we show the results for Ni-Au alloys, which are particularly important at the present time, as this is the only fcc metallic alloy for which there is EXAFS data over the whole range.[18] This alloy was chosen for the first EXAFS study because the length mismatch between Ni and Au is about 15%, which is around the upper limit for forming solid solutions.[19] The EAM results are good for all the partial length distributions and clearly superior to the CFM. Note that some of the error bars on the EXAFS results are quite large. Note also that the EAM and CFM give bowing of *opposite* sign for the mean length. The difference between these two sets of results, suggests that charge transfer effects are significant in Ni-Au alloys. The agreement obtained here between experiment and EAM is good. The large experimental uncertainties at low Ni concentration cannot discriminate between the EAM and the results with the Morse potential, used by Renaud *et al.*,[18] but the Morse potential gives a crossing of the Ni-Ni and Ni-Au curves which is perhaps less acceptable than our results. Comparing with earlier EAM simulations by Ackland and Vitek,[17] using the Finnis-Sinclair model for Cu-Au and Au-Ag, and Foiles[6] using the Daw-Baskes model for Cu-Ni, we see that the overall behavior of the Johnson EAM potential produces a smoother variation of the lattice constant with concentration.

In Figs. 7–9 we show only the more successful of the EAM and CFM results for each alloy, as determined by comparison with the diffraction data. In all nine cases shown, one method was clearly superior to the other. Surprisingly, when examining our results in Figs. 1–9, the CFM is superior to the EAM in at least as many cases as the EAM is superior to the CFM. Table II also shows that there is no clear preference for one approach over the other, which was of considerable surprise to us. With alloys containing platinum, the Johnson EAM potential does not give the right curvature for the mean length. Johnson already showed that his potential is weaker for Pt. It seems that the crude electronic model used in the embedded-atom method is not sufficient for platinum. But surprisingly, we found that the CFM (with no adjustable parameters) is in very good agreement with the mean experimental nearest-neighbor distance for all but one alloy for which the embedded-atom potential fails (see Table II). In Figs. 8 and 9, the simulations using the CFM and the diffraction results for the Pt-Ag, Pt-Au, Cu-Pt, and Ni-Pt are shown. There are small discrepancies for the Ni-Pt alloy, although the curvature is negative, the same as in the experimental results. For Pd-Pt, shown in Fig. 4, the CFM does *not* give better agreement with experiment than the EAM potential,

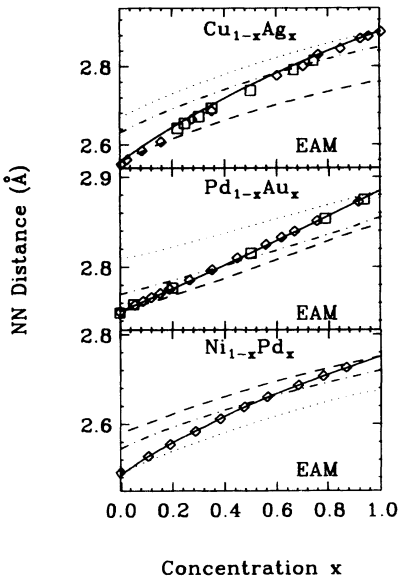

FIG. 7. Showing the EAM results for $Cu_{1-x}Ag_x$, $Pd_{1-x}Au_x$, and $Ni_{1-x}Pd_x$ in the three panels. In all cases, we show only the EAM results which were clearly better than the CFM results when compared with diffraction data (Refs. 23, 25–27).

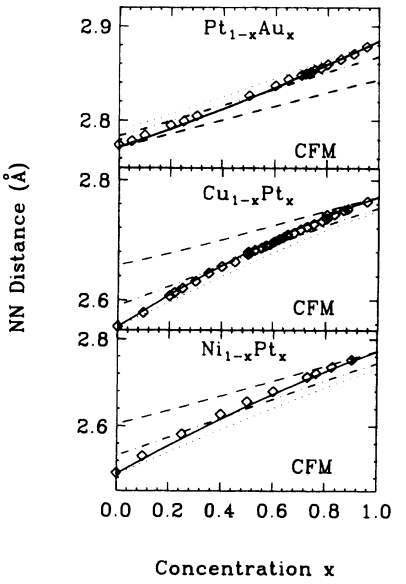

FIG. 9. Showing the CFM results for $Pt_{1-x}Au_x$, $Cu_{1-x}Pt_x$, and $Ni_{1-x}Pt_x$ in the three panels. In all cases we show only the CFM results which were clearly better than the EAM results when compared with diffraction data (Ref. 23).

both having the *wrong* sign for the deviation from Vegard's law. Figure 8 shows CFM simulations for Ni-Cu and Pd-Ag, which we see agree with the experimental data. It has been shown that semiconductors can be described analytically by a simple harmonic spring model (with angular forces)[16] because they approximately obey Pauling's rule of additivity of atomic radii, as expressed in Eq. (8). Our results would suggest that platinum alloys also respect the Pauling rule with no or little anharmonicity in the potential.

A selection of our results for the elastic constants are shown in Fig. 10; experimental elastic data for alloys are virtually nonexistent. But the smooth, rather uninteresting, behavior in every case might lead us to suppose that they are not too far from the real behavior, especially as the CFM and EAM give very similar results. The relation $C_{11} = C_{44} + C_{12}$ holds for every concentration x

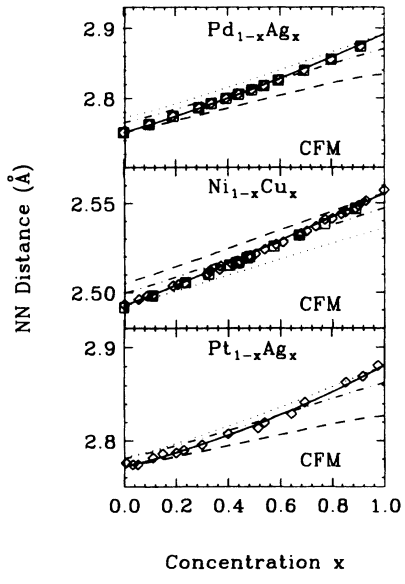

FIG. 8. Showing the CFM results for $Pd_{1-x}Ag_x$, $Ni_{1-x}Cu_x$, and $Pt_{1-x}Ag_x$ in the three panels. In all cases we show only the CFM results which were clearly better than the EAM results when compared with diffraction data (Refs. 28, 29, 22, and 30).

TABLE II. Alloys for which the EAM or the CFM gives the lattice parameter in agreement with experimental diffraction results (shown by a bullet). The crosses indicate disagreement with experimental results and the blanks indicate that no experimental data was available. The third column refers to the figure number(s) in this paper where the results are shown.

Alloy	EAM	Central force	Fig.
Au-Ag	•	×	1, 10
Cu-Ag	•	×	7
Pd-Ag	×	•	8
Cu-Au	•	•	2
Ni-Au	•	×	6, 10, 11
Pd-Au	•	×	7
Ni-Cu	×	•	8
Cu-Pd	•	•	3
Ni-Pd	•	×	7
Pt-Ag	×	•	8, 10
Pt-Au	×	•	9
Cu-Pt	×	•	9
Ni-Pt	×	•	9
Ni-Ag			5
Pd-Pt	×	×	4

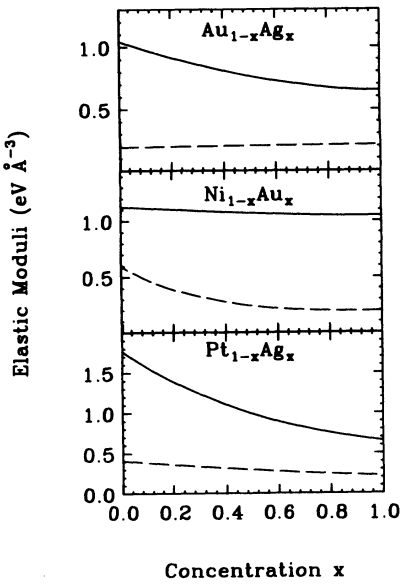

FIG. 10. The bulk modulus (solid line) and the Voight shear modulus (dashed line) for three different alloys obtained from the computer simulation with the EAM potential as described in the text.

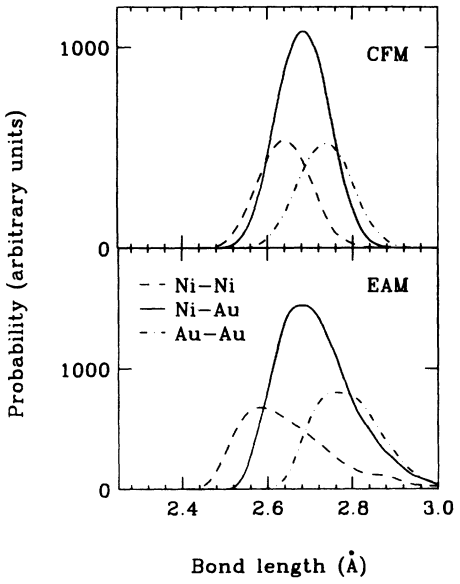

FIG. 11. The bond-length distributions for Ni-Ni, Ni-Au, and Au-Au nearest-neighbor distances in an $Ni_{0.5}Au_{0.5}$ alloy, computed using both the CFM (with no variation in the force constants) and the EAM.

within the limits of the precision on the numerical calculations using EAM for the alloys. In Fig. 10 we show the bulk modulus and the Voight average shear modulus, computed using the EAM. The results for the pure metals are exact as they were used as input in determining the parameters in the EAM. Computing the bulk modulus with both the spring model and the EAM potential, we find that its behavior is not very sensitive to the model used, and well described by the simple effective medium theory as given by (16). This effective medium approach must be applied separately to the bulk and shear moduli by fitting the end points via K_{AA} and K_{BB}. Note that the effective medium theory is designed to get the correct initial slope for small x and $1-x$.[14,16] We find also that the behavior of the elastic constant is very different from that determined by Ackland and Vitek.[17] Our calculation shows no change of curvature with the concentration in any of the alloys studied in this paper, as they observed for Cu-Au. Some experiments would be useful here.

Figure 11 shows the bond-length distribution for the CFM with *all the force constants equal* and for the EAM potential. The CFM with equal spring constants can be solved exactly to give the result (15) for the widths, in agreement with the simulation results shown in Fig. 11. The widths for the three peaks for the CFM in Fig. 11 are all equal and indeed the shapes are all similar apart from a vertical scale factor.[16] The CFM results are rather different from the EAM results, but have the important common feature that the widths are comparable to the peak separation. The full width at half the maximum, compared to the peak separation $< L_{BB} > - < L_{AA} >$ is given by

$$2\left[x(1-x)\ln 2\left(\frac{1-a^{**}}{a^{**}}\right)\right]^{1/2}, \qquad (17)$$

where we have used Eqs. (13) and (15). The lattice enters through the topological rigidity a^{**}. At $x=\frac{1}{2}$ the ratio (17) is much larger for metals, $\simeq 1.48$, than for semiconductors, $\simeq 0.18$, where a similar relation exists,[2] so that the length distributions are wide in the metal alloys studied here as seen in Fig. 11. In semiconductors the component peaks are more separated. These results make it very hard to justify using any virtual crystal type of approximation for the electronic properties of alloys, even at the crudest level.

VI. CONCLUSION

Our work gives no clear result in determining as to whether the central force model (CFM) or the embedded-atom method (EAM) is superior. For platinum alloys and a few others, the CFM is clearly superior, but in all other cases the EAM is better. This may be related to the amount of charge transfer in the alloy. We find that the Johnson EAM is very successful in Ni-Au alloys; the only case in which EXAFS data is available. The surprising contraction of the Au-Au bond in Ag-rich Au-Ag alloys within the EAM, points out that more *ab initio* calculations are needed for both single and pair *defects* in metals. Armed with this information, it will be possible to construct EAM potentials that will interpolate over the whole concentration range. In the absence of such calculations, the present results can be taken as a guide, but with a good deal of skepticism. The CFM explains why the widths of the length distributions are so wide, when compared to semiconductor alloys. This is because the fcc metal lattices have a topological rigidity parameter $a^{**} \simeq 0.24$ as compared with semiconductors where $a^{**} \simeq 0.8$. The width of these distributions means that the virtual crystal approximation is particularly in-

appropriate in metallic alloys.

The effect of charge transfer is important in many cases and is taken into account by the embedded-atom-method potential and is sufficient in many cases to give the correct variation of the lattice parameter with the concentration for most alloys, not containing Pt. The elastic constants show monotonic behavior with the concentration, and seem to be insensitive to the model used.

ACKNOWLEDGMENTS

We should like to thank J. Chen and R. A. Johnson for useful discussions. This work was partially supported by the NSF under Grant No. DMR 9024955. One of us (N.M.) is grateful to Natural Sciences and Engineering Research Council of Canada for partial support.

APPENDIX A: THE DILUTE LIMIT

In Sec. III, we consider a model where the spring constants for the three types of bonds—K_{AA}, K_{AB}, and K_{BB}—are the same. However, it is possible to solve the more general case of different spring constants in the dilute limit. In this limit (small x), we can rewrite the mean length

$$\langle L\rangle = (1-x)^2\langle L_{AA}\rangle + 2x(1-x)\langle L_{AB}\rangle + x^2\langle L_{BB}\rangle \tag{A1}$$

as

$$\langle L\rangle = (1-2x)\langle L_{AA}\rangle + 2x\langle L_{AB}\rangle. \tag{A2}$$

We have now only two types of bonds and two spring constants: K_{AA} and K_{AB}. We can therefore modify the solution to the dilute limit obtained by Thorpe, Jin, and Mahanti[31] in the random-bond case.

The equation for the average AB length is then,

$$\langle L_{AB}\rangle = L^0_{AA} + \left(1-(1-2x)\frac{K_{AA}(1/a^{**}-1)}{[K_{AA}(1-/a^{**}-1)+K_{AB}]}\right) \times (L^0_{AB}-L^0_{AA}). \tag{A3}$$

Setting $K_{AA}=K_{AB}=K$, we are back to Eq. (14), which is valid for any x.

[1] M.F. Thorpe and E.J. Garboczi, Phys. Rev. B **42**, 8805 (1990).
[2] Y. Cai, N. Mousseau, and M. F. Thorpe (unpublished).
[3] L. Vegard, Z. Phys. **5**, 17 (1921).
[4] M.S. Daw and M.I. Baskes, Phys. Rev. B **29**, 6443 (1984).
[5] M.W. Finnis and J.E. Sinclair, Philos. Mag. A **50**, 45 (1984).
[6] S.M. Foiles, Phys. Rev. B **32**, 7685 (1985).
[7] R.A. Johnson, Phys. Rev. B **37**, 3924 (1988).
[8] R.A. Johnson, Phys. Rev. B **39**, 12 554 (1989).
[9] R.A. Johnson, Phys. Rev. B **41**, 9717 (1990).
[10] Y. Cai and M. F. Thorpe (unpublished).
[11] G. Fournet, J. Phys. Radium **14**, 374 (1953); J. Friedel, Philos. Mag. **46**, 514 (1955).
[12] K.W. Jacobsen, Comments Cond. Mat. Phys. **14**, 129 (1988).
[13] S. Feng, M.F. Thorpe, and E. Garboczi, Phys. Rev. B **31**, 276 (1985).
[14] M. F. Thorpe and W. Tang, J. Phys. C **20**, 3925 (1987).
[15] J. Chen and M. F. Thorpe (unpublished).
[16] Y. Cai, J. S. Chung, M. F. Thorpe, and S. D. Mahanti, Phys. Rev. B **42**, 8827 (1990).
[17] G.J. Ackland and V. Vitek, Phys. Rev. B **41**, 10 324 (1990).
[18] G. Renaud, N. Motta, F. Lançon, and M. Belakhovsky, Phys. Rev. B **38**, 5944 (1988).
[19] W. Hume-Rothery, *Electrons, Atoms, Metals and Alloys* (Cassies Co., London, 1948).
[20] L. Karmazin, Czech. J. Phys. **19**, 634 (1969).
[21] J.O. Linde, Ann. Phys. (Leipzig) [Folge 5] **15**, 249 (1932); F.C. Nix and D. Macnair, Phys. Rev. **60**, 597 (1941); J.B. Newkirk, J. Metals **5**, 823 (1953).
[22] F. Lihl, H. Ebel, and W. Baumgartner, Z. Metallkd. **62**, 42 (1971).
[23] W.B. Pearson, *Handbook of Lattice Spacing and Structure of Metals and Alloys* (Pergamon, New York, 1958).
[24] J.B. Darby and K.M. Myles, Metall. Trans. **3**, 653 (1972).
[25] S. Nagakura, S. Toyama, and S. Oketani, Acta Metall. **14**, 73 (1966).
[26] A. Mealand and T.B. Flanagan, Can. J. Phys. **42**, 2364 (1964).
[27] L.R. Bidwell, Acta Crystallogr. **17**, 1473 (1964).
[28] B.R. Coles, J. Inst. Metals **84**, 346 (1956).
[29] E.A. Owen and L. Pickup, Z. Kristallogr. Kristallgeom. Krystallphy. Kristallchem. A **88**, 116 (1934); B.R. Coles, J. Inst. Metall. **84**, 364 (1955/56).
[30] C.H. Johansson and J.O. Linde, Ann. Phys. (Leipzig) **6**, 458 (1930); **7**, 408 (1930); O.A. Novikova and A.A. Rudnitskii, Zh. Neorg. Khim. **2**, 1840 (1957); W. Klement, Jr., and H.L. Luo, Trans. Metall. Soc. AIME **227**, 1253 (1963); H. Ebert, J. Abart, and J. Voitländer, J. Less-Common Met. **91**, 89 (1983).
[31] M. F. Thorpe, W. Jin, and S. D. Mahanti, Phys. Rev. B **40**, 10 294 (1989).